THE USE OF A TRANSPARENT AQUEOUS ANALOGUE TO DEMONSTRATE THE DEVELOPMENT OF SEGREGATION CHANNELS DURING ALLOY SOLIFICIATION, VERTICALLY UPWARDS

R. S. Steube and A. Hellawell
Dept. of Metallurgical and Materials Engineering
Michigan Technological University
Houghton, MI 49931

ABSTRACT

The consequences of thermo-solutal convection during alloy solidification are demonstrated in a compilation of video recordings of analogous behavior in the transparent system, NH_4Cl-H_2O. The visual illustration is in five parts concerned with (1) general procedure, (2) the start of plume convection, (3) plume characteristics and interactions, (4) channel/plume correlation and particulate transport, and (5) channel detail and propagation. Wherever possible, attention is drawn to parallel behavior in the aqueous and an organic system with that thought to take place in opaque metallic systems. Extrapolation between the convection in metallic, aqueous and organic systems is briefly discussed.

I. INTRODUCTION

This is a phenomenological description and illustration of convection patterns which arise from thermo-solutal density gradients. During the solidification of metallic samples which freeze relatively slowly (times in a range of 10^3-10^4 s) over a temperature range, local, nearly vertical segregation channels can develop in the solid-liquid "mushy" region, having widths of <2 mm and lengths >100 mm. These channels appear in a fully solidified ingot as pencils of higher solute concentration, internally or on the outer surface, and may be distinguished by having a polycrystalline structure within a matrix which is either a single crystal or consists of aligned columnar grains. Figure 1 shows an example of channels formed in a maraging alloy steel (Mar M200) ingot, solidified vertically from below, after heavy etching. The figure shows long, vertical columnar grains of varying

contrast, while segregation channels appear as columns or "pipes" showing the fine polycrystalline structure, similarly revealed by orientation dependent reflection. The solute concentration within these channels is a few percent (e.g., 1 wt.% to 3 wt.%) higher than elsewhere, predominantly of those components which are less dense than the base solvent, e.g., Sn or Sb in Pb; C, Si, S or P in Fe. The microstructures within the channels typically reveal higher proportions of eutectic material: Fig. 2(b) is an example taken from a Pb-Sb ingot and Fig. 2(a) shows the corresponding concentration profile across the channel. Such features are regarded as serious foundry defects and their presence generally requires the rejection of a casting.

The origin of these channels has been identified as convection patterns which arise in the partly solidified material from competition between thermal and solutal density variations within the system, hence thermo-solutal convection [MacDonald and Hunt,[1,2] Copley et al.[3]]. The situation may be understood with reference to Figs. 3(a)-(d). In a phase diagram of the form of Fig. 3(a), an alloy of bulk liquid composition, C_o, is freezing vertically upwards and has developed a "mushy region," Fig. 3(b). The solidifying material lies in a positive, vertical temperature gradient, so that the mushy region extends from a dendritic growth front down to the eutectic temperature of the corresponding phase diagram, Fig. 3(a), below which it is fully solid. Immediately above the dendritic front there is a solute boundary layer in which the solute concentration rises from that of the bulk, C_o, to C_L, where the liquid is in local equilibrium with solid dendrite tips of concentration C_d. The ratio of the concentrations, C_d/C_L, is the solid-liquid distribution coefficient, k_o, which is a constant if the liquidus and solidus lines are straight. The horizontal broken lines between Figs. 3(a) and (b) relate the vertical height in the positive temperature gradient, dT/dz, to temperatures and compositions on the phase diagram. Figure 3(c) shows the vertical liquid and solid composition profiles corresponding to Figs. 3(a) and (b): the bulk liquid composition is constant, C_o, but close to the growth front the liquid composition rises ahead of dendrite tips to C_L, while the interdendritic liquid composition continues to rise below the plane of the growth front within the "mushy region." Assuming local solid-liquid mixing by diffusion at any level, the vertical

interdendritic liquid gradient is given by $dc/dz = dc/dT \times dT/dz$. Then, Fig. 3(d), above the immediate level of the growth front, the bulk liquid density decreases upwards according to the coefficient of volume expansion, α, and the temperature gradient; $d\rho/dz$ is negative in this region and the bulk liquid is stabilized against convection. Disregarding the local lateral variations close to dendrite tips, the interdendritic liquid then has a density gradient which is determined by both the thermal and solutal coefficients of expansion. If the solutal coefficient, β, is negative (solute less dense) and sufficiently exceeds the thermal coefficient, α (as is frequently the case), then the density of the interdendritic liquid decreases down the liquidus line on the phase diagram and density inversion occurs, as shown in Fig. 3(d). Moreover, if the positive density gradient below the plane of the front exceeds that of the negative gradient above, again, as in Fig. 3(d), there will be a resultant buoyancy force available to drive any convective perturbation, i.e., when $\beta\, dc/dz > -\alpha\, dT/dz$ [e.g., Sharp and Hellawell,[4] Coriell et al.,[5] Hurle et al.[6]].

In opaque metals, there are, as yet, no methods to observe what happens during solidification and all information is post mortem, as in Figs. 1 and 2. Therefore, extensive use has been made of transparent systems to simulate such solidification behavior, in particular, using the aqueous system with NH_4Cl, Fig. 4, which exhibits a suitable liquidus slope (-5 K/wt.% H_2O). NH_4Cl solidifies from the aqueous solution with a dendritic morphology; it has a cubic crystal structure, as do a majority of metals; and the solute, water, is the less dense. The liquid density along the liquidus line decreases with temperature, i.e., $\beta\, dC/dz > -\alpha\, dT/dz$. The thermal conductivity of aqueous solutions is much lower than those of metals, so that the Prandtl numbers ($\eta/\kappa\rho$) differ by some two orders of magnitude (liquid metals $\sim 2 \cdot 10^{-2}$; NH_4Cl-H_2O ~7). The experimentally feasible composition range in the aqueous system lies around 70 wt.% H_2O, Fig. 4, and in this range the dendritic solid fraction in the mushy zone is typically much less than it is in those parts of metallic systems where channels form. However, these differences combine to allow the development of segregation channels in the aqueous system which are remarkably similar in scale and structure to those found in metallic ingots. The system therefore appears to be a very good analogue for the metallic behavior of interest, and a significant solutal

dependence of the refractive index allows it to be used for a visual illustration of how segregation channels form and propagate.

As convection is a dynamic effect, single frame pictures can do only partial justice to what can be seen directly, so that a video recording provides a much more convincing demonstration of the phenomenon. In the following, we describe alternative illumination systems which have been used to view different aspects of interest and then comment on a number of excerpts from video recordings which illustrate points which are thought to be particularly relevant to metal castings.

II. PROCEDURE

The geometrical configuration of the experiments is as shown schematically in Fig. 3(b). The essential optical arrangement is as shown in Fig. 5. The central cell or mold consists of open-ended glass tubing of square or rectangular section (50 mm × 50 mm or 30 mm × 50 mm), typically 250 mm in height, mounted and sealed with silicone grease onto a copper base. Into this clean, dust-free mold is poured a hot aqueous solution at a measured temperature. The solution is prepared from distilled water and analar salt and is passed, hot, through <1 μm mesh filter prior to pouring. The mold may be preheated above the liquidus temperature and the copper base may be prechilled or cooled after pouring by immersion in a Dewar containing liquid nitrogen (-195°C) or solid CO_2 and ethanol (-76°C). Fine thermocouples may be immersed or inserted into the mold contents, and continuously record vertical and horizontal temperature variations. The entire mold assembly can be moved vertically and horizontally with respect to the optical system. Bulk liquid and plume composition have been recorded during experiments by sampling with a hypodermic needle and using refractive index to measure composition [Sarazin et al.[7-10]].

The illumination is effected by one or two 300 watt fiber-optic sources, or by a collimated or divergent laser beam of width ≈0.5 mm. Two sources of contrast exist: either, with observation at right angles or acutely to the transmitted illumination, light scattered by (crystalline) fragments may be recorded against a relatively dark field; or, with diffuse or oblique illumination, contrast arises from local variations in refractive index with a relatively light field. In the former, it should be explained that at various times the

liquid inherently contains a dispersion of dendrite fragments, many of which survive and grow into equiaxed dendritic crystals, exhibiting characteristic orthogonal shape. Alternatively, or additionally, insoluble particles, such as near-isodensity latex spheres, may be introduced into the system. Light scattered by such dispersions allows their movements to be followed over distances >10 mm, or their presence to be detected in limited volumes by scintillations. The limit of resolution, **d**, involves the usual optical compromise with magnification and depth of field, **h**, governed by the numerical aperture. In the present assembly, with binocular, zoom and monitor configurations, the limits of the system lie between $\mathbf{d} \approx 2.5$ μm with $\mathbf{h} \approx 0.25$ mm to $\mathbf{d} \approx 100$ μm with $\mathbf{h} \approx 12.5$ mm at corresponding magnifications between 282× and 10×. These values are for operation in air; in a convecting liquid, with mold walls of slightly variable thickness, they would be optimistic. On the other hand, in the light scattering, scintillation mode, using a LASER beam source, particles are detectable as point sources with dimensions far below those which are normally physically resolvable. The detection limits are then primarily determined by total source intensity, i.e., number of photons reflected. Thus in a thin plane of intense illumination, viewed in a dark field, only the scintillations are recorded as fragments pass through that plane, and the dimensions of those reflecting sources are not clearly evident. This is truly "dark field." The significance of the limitations of the depths of field and resolution can be better appreciated from the video recording, which reveals the need to make frequent adjustments to the location of relevant events.

Refractive index contrast may be utilized in two ways. Referring to Fig. 5, light from a divergent point source may be used in transmission by direct observation (as in the present work) or by projection onto a translucent screen, A (this is the Schlieren technique). Alternatively, a wider divergent light source may be used to illuminate a translucent screen, B, placed before the cell. Viewed in transmission, this diffuse illumination then produces "solid" images by light scattering at positions where there are sharp discontinuities in the gradient of refractive index. Convective plume images obtained in this manner are here referred to as "light field."

In the NH_4Cl-H_2O system, the solutal refractive index coefficient is $\approx 2 \cdot 10^{-3}$ wt.%$^{-1}$, nearly an order of magnitude greater than the corresponding thermal coefficient, K^{-1}.

Thus, with discontinuities of 1-2 wt.% in composition or 1-2 K, the contrast is dominated by composition. It may be noted here that in the NH_4Cl-H_2O system, convective plumes are water-rich, so that light passing through a plume is divergent or effectively scattered when viewed in the light field mode. Limits of resolution by this technique are probably sensitive to discontinuities of ~± 0.1 wt.% H_2O. In an alternative transparent system, such as that of succinonitrile (SCN)-ethanol (EtOH), the solutal coefficient of refractive index is only about a quarter of that in the aqueous system and the contrast is correspondingly weaker.

Finally, it is, of course, possible to introduce color contrast, as by the insertion of $KMnO_4$ crystals into the system at some point.[2] This method may give good steady-state contrast but is difficult to control, and can only be qualitative at best.

In the tape recordings, all of these types of contrast will be evident, and in some cases there are subtle (accidental) combinations of these, obtained during exploratory adjustments of the illumination.

In the recordings, frames are of duration 1/30 s. "Stills" from individual frames may then be photographed from the screen directly, be transformed by an image analysis system, or be electrostatically reproduced by a "frame grabber" system.

III. RESULTS: VIDEO RECORDS

Band 1 (36 seconds): General Procedure

Band 2 (102 seconds): Plume Evolution

Band 3 (140 seconds): Helical Flow and Interactions

Band 4 (60 seconds): Channel-Plume Activity

Band 5 (80 seconds): Channel Details

Band 1: General Procedure (36 seconds)

This introductory section shows the initial pouring operation, followed by chilling of the base of the mold with liquid nitrogen, and the subsequent establishment of a solid-liquid mushy region lying between supernatant solution above and fully solidified material below the eutectic temperature of -16°C (Fig. 4). The sequence concludes with a general view of convective solute plumes, rising from cones at channel "mouths" and

illustrating the quasi-steady state situation which develops in about one hour after the pour and chilling operations. After such a time, the general, global arrangement is as shown schematically in Fig. 6, in which are indicated various relevant dimensions of interest. Macroscopic dimensions may be assessed on the tape from an adjacent scale, inset beside the mold. Typically, values for the plume radius would be $r < 0.5$ mm, and for channel/ plume spacings, L, from 5 mm to 10 mm.

Conditions are, of course, changing continuously during such an experiment over a period of some three hours. The entire assembly is cooling, mostly by abstraction of heat through the copper base, but this becomes progressively slower as the depth of poor conducting salt and ice increases. At the same time, ejection of water-rich liquid by the plumes causes the bulk liquid composition to rise (in H_2O) and the freezing point to fall, so that solidification is incomplete unless a short (e.g., 10 cm) mold is used. The exact details also vary with pouring temperature, but as an example, Fig. 7 shows the positions of the dendritic and eutectic fronts vs. time after pouring a solution of 70 wt.% H_2O, from a temperature ~30 K above the liquidus. Fig. 7 shows that as the height of the fully solid region increases, poor heat flow through this mixture of NH_4Cl and ice retards the rate of solidification, while the mushy region settles to a depth, D, Fig. 6, around 35 mm. The initial fall and subsequent rise in the level of the bulk liquid meniscus reflects the earlier contraction on solidification of NH_4Cl, which is gradually counteracted by the expansion on forming ice. Ice is the major phase in the fully solidified eutectic material. An example of corresponding composition changes, close ($\approx$20 mm) to the dendritic growth front, is also shown in Fig. 8, for bulk, ●, and for plume composition, ■, as functions of time after pouring. As an experiment proceeds, both compositions increase and also gradually converge, so that the buoyancy contribution within a plume falls and convection gradually dies away to slow plume flow from one or two surviving channels. The temperatures of plume liquid may simultaneously be recorded by means of fine thermocouples; typically, in the aqueous system, ejected liquid at channel mouths is some 3 K - 4 K cooler than that of the surrounding bulk, warming up to the ambient temperature at some 100 mm above the front, or, with mean plume flow rates of 6 mm s^{-1} to 8 mm s^{-1}, within less than 20 s. While

all the video record shown here relates to the aqueous system, parallel studies have also been carried out with the organic system, SCN-EtOH, having a Prandtl number around 20, and results for these two transparent systems have been compared with post mortem measurements on metallic samples. The overall plan has been to analyze the observations made with the transparent systems and to extrapolate these to make predictions of flow rates in metals which could not be observed directly. The outcome of this comparison is briefly discussed in Section IV.

Band 2: Plume Evolution (102 seconds)

Given the necessary density inversion, thermo-solutal convection begins within a few minutes of the formation of a dendritic growth front. The initial pattern is not one of well-defined channel/plumes but rather of short range, fluctuating "fingers," on a lateral scale similar to that of the primary interdendritic spacing (e.g., 0.3 mm) and extending some 5 mm above the front. This finger regime appears on the tape with essentially light field contrast and it may be seen that the upward and concomitant downward flows are not well synchronized, giving, rather, an appearance of local, short range turbulence. After about 10^3 s, some finger movements are seen to extend locally into the overlying, quiescent body of liquid, and a few of these rapidly reinforce to develop a longer range plume. As the plume evolves over a 10-20 s period, a channel develops in the mushy zone below and quasi-steady state plume flow becomes established, with necessary local circulation and re-entrainment to sustain the upward flow. As more plumes and channels develop, apparently at random positions, the finger activity wanes and nearly all convection is concentrated into weakly interacting plumes.

It follows that the gradual composition change in the bulk liquid correlates well with estimates of the total volume of water transported away from the growth front in plumes. The mass balance is necessarily maintained in this way.

The coupling required to establish plume flow of this type involves not only that between fingers and the overlying, quiescent body of liquid, but also between the boundary layer region and the interdendritic liquid below. It is the porous nature of the mushy region which allows re-entrainment of the bulk liquid, and at a solid, planar growth front such recirculation would not be possible. The plume compositions and temperatures indicate

that the fluid rising does not originate at depths in excess of ≈5 to 8 mm below the growth front itself i.e., comparable with interchannel spacings or equivalent to about 10 channel diameters). In any event, the development of a liquid perturbation precedes the release of interdendritic liquid and channels are a consequence of these events in the immediate vicinity of the dendritic front, Fig. 9, rather than an eruption at some depth within the mushy region, as had been sometimes suggested [Bridge et al.,[11] Voller et al.,[12] Simpson et al.[13]]. Similar observations and relevant discussions are to be found elsewhere in the literature [e.g., Bennon and Incropera,[14] Chen and Chen,[15] Huppert,[16] Magirl and Incropera,[17] Felicelli et al.[18]].

Band 3: Helical Flow and Plume Interactions (140 seconds)

It will have already been apparent from preceding bands that plume flow, although essentially streamlined at any one level, does not maintain exact vertical alignment along its entire length. In the aqueous system, although not in the more sluggish organic system, plumes acquire a sinuous pattern as their height increases and appear from the side view to wave about laterally. Viewed obliquely, it becomes apparent that the plume form is actually helical and this is clearly evident if the cell is viewed from above, through a prism, one face of which is beneath the meniscus. In the video record, this helical motion is emphasized by coloring the solution with potassium permanganate, introduced as small crystals close to the channel mouths, at the growth front. General inspection reveals that the sense of the helices is both left and right handed, although this can be deceptive from a side view alone. In the video, the top view of the central plume shows an example in which the sense of precession is right handed with respect to the axis of vertical flow.

The motion is reminiscent of that sometimes seen in smoke columns, rising in still air. The reason that the plumes wave about when viewed from the side is that the helices are rotating about their vertical axes in a sense which is opposite to the thread of flow within the plumes. Thus a right handed thread rotates clockwise as seen from above, and vice versa. The frictional loss of plume vs. bulk liquids at the plume walls is responsible for this counter rotation, which in turn accounts for the illusion that the entire plume is moving upwards. Actually, flow around the helical thread within a plume is always more

rapid than the rise associated with the rotation; were it not so, the plume liquid would not keep up with the helical motion and the direction of flow would be downwards!

A correlation between plume flow rates, the pitch and counter revolution of helices has been made elsewhere [Sarazin et al.[10]]. As far as the channel patterns are concerned, left behind in the mushy zone below, these plume convolutions are not important, being confined to levels well above that of the growth front. They are instructive, however, in that adjacent plumes interact sufficiently for their helices and rotation rates to become, at times, remarkably synchronized, as tape examples illustrate. It may further be seen on close inspection that the rotation causes the plume sections to become distorted into airfoil shapes with leading and trailing edges. As previously mentioned, such motion is not observed in SCN base systems where flow rates are nearly an order of magnitude slower. In the latter case, plumes rise straight and vertically, breaking down by Raleigh-Taylor perturbations into globules of solute-rich fluid, before any helical motion develops. At present, there is no means of knowing if such patterns occur in liquid metals.

Band 4: Channel-Plume Activity (60 seconds)

In this sequence, the region close to a channel mouth is examined in more detail using light and dark field illumination. Typically, the plumes which are illustrated are somewhat less than 1 mm in diameter. It will have been noticed from previous bands that as plumes become established, the concomitant channel exit rapidly develops a conical rim of dendrites, rather like a volcanic cone. This feature can also be detected in metallic alloys at the growth front of quenched samples [Sarazin[7]], but is hardly perceptible in the more sluggish organic system. The development of this rim may be attributed to the fact that, as bulk liquid is entrained between channels and recirculates within the upper levels of the mushy region, it is cooled by a few degrees before being ejected as a plume, so that the dendritic front advances locally, with local temperatures a little below the general level of the front. It may also be seen occasionally that falling crystal fragments are caught up in the re-entrainment process and are incorporated in the mushy zone as randomly oriented "stray" crystals.

In the light field images, the primary contrast is from the compositional discontinuity at the plume "walls." The composition profile across a plume will be

essentially of square wave form, because the plume flow rate is much too rapid to allow of significant lateral solute redistribution. On the other hand, the corresponding velocity profile will be smeared out as some of the surrounding liquid is drawn up by the core of the plume. A possible velocity profile across a plume may then be parabolic within the "walls" and exponential without, Fig. 10. It will be noticed that while there is little other contrast, apart from the silhouette of the dendritic cone, there are occasional large, dark fragments of the dendritic mesh carried up in the plumes. The distribution of these and smaller fragments, and also the overall flow pattern, are seen much more clearly in the dark field images.

In the video record, general dark field images show the ejection of dendritic fragments from a channel mouth and also falling or returning crystals which have survived at higher levels and have grown as they sank back onto the growth front. The occasional re-entrainment of such a crystal gives a good idea of the stream flow around a plume. An estimate of the number of resolvable (i.e., ≈40 μm) ejected fragments from a "typical" active channel mouth is around 8 s^{-1}. With a "typical" density of channel-plumes ≈ $2 \cdot 10^3$ m^{-2}, this is equivalent to a number of ≈$1.6 \cdot 10^4$ m^{-2} s^{-1} particles being injected into the "open" supernatant liquid. Of course, not all of these crystal fragments survive. A majority must melt until the bulk liquid cools below the liquidus temperature. Nevertheless, were all these fragments to survive, it will be appreciated that within, say, 1000 s, the population density in 1 m^3 of "open" melt would be ≈$1.6 \cdot 10^7$ m^{-3}. The importance of these estimates in determining the development of grain structure in a casting becomes self-evident, and it will be realized that this inherent source of equiaxed crystal nuclei is a determining factor controlling the columnar to equiaxed transition in grain structure [e.g., Steube and Hellawell,[19] Prescott et al. [20]].

Band 4 concludes with a brief section in which a channel mouth is illuminated by a LASER beam of width 0.5 mm. This shows a truly dark field image in which crystal fragments scintillate as they pass through the beam. This is significant in that it provides a technique to obtain more precise quantitative information which, in turn, is intended to provide a basis for modelling the grain structure of castings. The dendrite fragments which

are ejected from channel mouths are formed by ripening and melting off of dendrite side arms, as has been observed in transparent organic materials (e.g., Jackson et al.,[21] Glicksman and Schaeffer.,[22] Sato et al.[23]]. The extent to which this fragmentation is assisted by convective flow within the mushy region is not yet clear, although, intuitively it might be expected that the process will accelerate and there is evidence that this is so [Paradies and Glicksman[24]].

Band 5: Channel Detail (80 seconds)

In general, the location of channels is apparently random, but shows a preference for those parts of a growth front which are higher than elsewhere, depending on the shape of the temperature isotherms within the mold. Some channels therefore develop at the mold walls and this band of the video record shows one of these. In effect, the view is of a half-channel or exploded section, which allows observation of detail below a channel "mouth." The illumination is from the front face of the mold and there is some coloration from a nearby crystal of potassium permanganate.

Convection from this channel was waning, but continued to show the ejection of dendritic fragments in the upper regions, close to the mouth. The aligned dendritic structure of the solid-liquid mushy region is clearly displayed, and coarsening and ripening of this array is evident below the channel cone. It may be seen that while fragments are ejected from the upper levels by the recirculation process, the channel liquid lower down, at depths around 10 mm, is more nearly quiescent. Dendrite fragments at this level are not ejected, but fall to a lower level and collect as randomly oriented debris, where they grow into small polycrystals within the surrounding columnar structure. Referring back to the metallic structure of Fig. 1, it will readily be understood how the polycrystalline structure of a channel developed the typical superficial appearance of a "freckle."

It can further be understood from the sequence in this band that the propagation of a channel at an advancing growth front is essentially maintained by local activity close to that front (depths comparable with the interchannel spacings) and that liquid at greater depths is relatively stagnant. Propagation of the channel and its convective activity is thus quite localized, but the structural damage left behind can extend almost indefinitely.

The video record concludes with enlarged detail of a superficial channel on the metallic sample, Fig. 1 of this text, showing the analogous polycrystalline structure to that which can be seen to develop in the transparent system.

IV. DISCUSSION

The preceding text and video record present a phenomenological description of a prominent aspect of thermosolutal convection which occurs during solidification. Reference has been made in the video commentary to parallel behavior between transparent and metallic materials, but a full discussion of the many points of interest which arise is beyond the scope of this presentation. We confined ourselves to two general observations.

First, the widths and spacings of channels/plumes are remarkably similar in different material, covering some three orders in Prandtl number. In order to understand why this might be, it is important to remember that this convective process is continuously driven by the phase transition which creates and maintains a more or less constant degree of density inversion. This drives the activity and, when solidification ceases, so does plume flow. Convective plumes may be likened to pipes, the lower ends of which are embedded in the dendritic mesh, so that the upward flow is restricted by the rate of re-entrainment which is possible through that mesh. The selection of channel/plume dimensions is therefore a compromise between the buoyancy of the less dense liquid and the rate at which a plume can be supplied. Analysis of interdendritic flow through a mesh of low solid fraction and variable geometry is a complex problem [e.g., Sample and Hellawell,[25] Ganesan and Poirier,[26] Ni and Beckermann[27]] but, approximately, the volume of liquid flowing up a plume increases with the radius, r, to the fourth power, while the number of interdendritic supply paths increases only with the channel circumference, $2\pi r$. Clearly, there is a physically restricted, upper limit beyond which adequate re-entrainment cannot be sustained and, other things being equal (buoyancy, viscosity, etc.), this may determine the observed operating dimensions.

Secondly, as explained above in section III, part 1, one object of this research has been to use the transparent materials to predict probable plume flow rates in liquid metals.

Although the channel/plume dimensions are similar in metallic, aqueous and organic systems, the flow rates are very different, those in the aqueous solution being an order of magnitude faster than in the organics (approx. <10 mm s^{-1} : ≈ 1 mm s^{-1}). Analysis of plume flow, referred to in section III, part 4, and Ref. 10, using post mortem data from metals to estimate buoyancy, would indicate that flow rates in metallic plumes are in excess of 100 mm s^{-1}. This may seem to be a somewhat dramatic conclusion, but it is not incompatible with estimates made for purely thermal convection in liquid metals, which are as high as 0.5 m s^{-1} [e.g., Gebhart et al[28]].

V. SUMMARY

The development and propagation of segregation channels has been described with reference to metallic, aqueous and organic systems covering a range of three orders of magnitude in Prandtl number.

A video record has been compiled from observations of ammonium chloride-water solutions to illustrate how thermo-solutal convection above a dendritic growth front leads to channel formation in the solid-liquid mushy region.

The propagation of segregation channels has been shown to take place by continuous re-entrainment of bulk liquid, through the upper part of the mushy zone, with ejection in the form of solute-rich, buoyant plumes. Attention is drawn to the importance of this form of convection as a mechanism for transporting dendritic crystal fragments from the mushy region into the bulk liquid. Such particulate dispersion is relevant to the development of the grain structure in metallic castings and the modeling thereof.

The selection of channel/plume dimensions is briefly discussed and extrapolation of analyzed flow rates between systems is outlined. It is estimated that plume flow rates in liquid metals exceed those in aqueous systems by an order of magnitude, and the latter are observed to exceed those in an organic liquid by a similar margin; to a first approximation, the flow rates are ≈ 100 mm s^{-1} : 10 mm s^{-1} : 1 mm s^{-1}.

ACKNOWLEDGEMENTS

This contribution is taken from a program of research into channel segregation which has been supported by NASA, through NASA-Lewis Research Center, Grant No.

NAG-3-560, and by the National Science Foundation, Division of Materials Research, Grants No. DMR-8815049 and DMR-9206783.

REFERENCES

1. R. J. McDonald and J. D. Hunt, *Trans. TMS-AIME*, **245**, 1993-1996 (1969).
2. R. J. McDonald and J. D. Hunt, *Metallurgical Trans.*, **A1**, 1787-1788 (1970).
3. S. M. Copley, A. F. Giamei, S. M. Johnson and M. F. Hornbecker, *Metallurgical Trans.*, **A1**, 2193-2204 (1970).
4. R. M. Sharp and A. Hellawell, *J. Crystal Growth*, **12**, 261-265 (1972).
5. S. R. Coriell, M. R. Cordes, W. J. Boettinger and R. F. Sekerka, *J. Crystal Growth*, **49**, 13-24 (1980).
6. D.T.J. Hurle, E. Jakeman and A. A. Wheeler, *J. Crystal Growth*, **58**, 163-171 (1982).
7. J. R. Sarazin, *Buoyancy Driven Convection and Channel Segregation during Solidification in Metallic, Aqueous, and Organic Systems*, Ph.D. Thesis, Michigan Technological University (1990).
8. J. R. Sarazin and A. Hellawell, *Metallurgical Trans.*, **A19**, 1861-1871 (1988).
9. J. R. Sarazin, R. S. Steube and A. Hellawell, in *Nature and Properties of Semi-Solid Materials*, ed. Sekhar and Dantzig, The Minerals, Metals and Materials Society, Warrendale, PA, pp.143-152 (1992).
10. J. R. Sarazin, R. S. Steube and A. Hellawell, in press, *Phil. Trans. Roy. Soc.*, A.
11. M. R. Bridge, M. P. Stephenson and J. Beech, *Metals Technology*, **9**, 429-433 (1982).
12. V. Voller, J. J. Moore and N. A. Shah, *Metals Technology*, **10**, 81-84 (1983).
13. M. Simpson, M. Verebakan and M. C. Flemings, *Metallurgical Trans.*, **A16**, 1687-1689 (1985).
14. W. D. Bennon and F. P. Incropera, *J. Heat and Mass Transfer*, **30**, 2161-2170 (1987).
15. F. Chen and C. F. Chen, *J. Fluid Mechanics*, **207**, 311-321 (1989).
16. H. E. Huppert, *J. Fluid Mechanics*, **212**, 209-240 (1990).

17. C. A. Magirl and F. P. Incropera, in *Topics in Heat Transfer*, vol. I, ASME–HTD, vol. 206, pp. 1-9 (1992).

18. S. D. Felicelli, J. C. Heinrich and D. R. Poirier, *Met. Trans. B*, **22**, 847-859.

19. R. S. Steube and A. Hellawell, in *Micro/Macro Scale Phenomena in Solidification*, ASME–HTD, vol. 218, pp. 73-83 (1992).

20. P. J. Prescott, F. P. Incropera and D. R. Gaskell, in *Transport Phenomena in Materials Processing and Manufacturing*, ASME–HTD, vol. 196, pp. 31-39 (1992).

21. K. A. Jackson, J. D. Hunt, D. R. Uhlmann and T. P. Seward, *Trans. Met. Soc. AIME.*, **236**, 149-160 (1966).

22. M. E. Glicksman and R. J. Schaeffer, *The Solidification of Metals,* Iron and Steel Inst., London, Book #110, pp. 43-48 (1968).

23. T. Sato, W. Kurz and K. Ikawa, *Trans. Japan, Inst. Metals*, **28**, 1012-1021 (1987).

24. C. J. Paradies and M. E. Glicksman, *Proceedings of the TMS Annual Meeting* (Denver, February 1993), Session: "Cast Shop III: Grain Refinement and Modification.," The Minerals, Metals, and Materials Society, Warrendale, PA (1993).

25. A. K. Sample and A. Hellawell, *Metallurgical Trans.*, **A15**, 2163-2173 (1984).

26. S. Ganesan and D. R. Poirier, *Metallurgical Trans.*, **B21**, 173 (1990).

27. J. Ni and C. Beckermann, *Metallurgical Trans.*, **B22**, 349 (1991).

28. B. Gebhart, Y. Jaluria, R. L. Mahajan and B. Samakia, *Buoyancy Induced Flows and Transport*, Chapter 1, Harper and Row, New York (1988).

FIGURES

1. Superficial "freckles" on a directionally solidified ingot (Mar M200), diameter ≈10 cm, courtesy A. F. Giamei, United Technologies, E. Hartford, CT.[3]
2. (a) Composition profile across a segregation channel in a Pb-2 wt.% Sb ingot, obtained by EMPA, and (b) detail of the channel microstructure, showing eutectic material and EMPA scanning traces corresponding to 2(a).[7,9,10]
3. (a) Portion of phase diagram; (b) schematic for sample of composition C_0, growing upwards; (c) corresponding vertical composition profile for (a) and (b), indicating bulk liquid composition, C_0, interfacial composition, C_L, and dendrite composition, C_d; and (d) thermal and solutal liquid density profile corresponding to (b) and (c).[3,8]
4. Relevant part of NH_4Cl-H_2O phase diagram, indicating composition range of interest.
5. Schematic plan of optical configurations used to provide video record.[9]
6. To indicate global dimensions relevant to the experimental procedure and analysis.[7,10]
7. Typical development of liquidus and eutectic heights at time after pouring into a chill base mold.[10]
8. Bulk and plume liquid compositions at time after pouring into the mold.[10]
9. Schematic representation of a perturbation leading to channel-plume convection.[23]
10. Schematic velocity profile through a plume of visible (composition) radius r_1, out to some limiting radius, r_2, with internal velocity V_1, and external velocity V_2.[10]

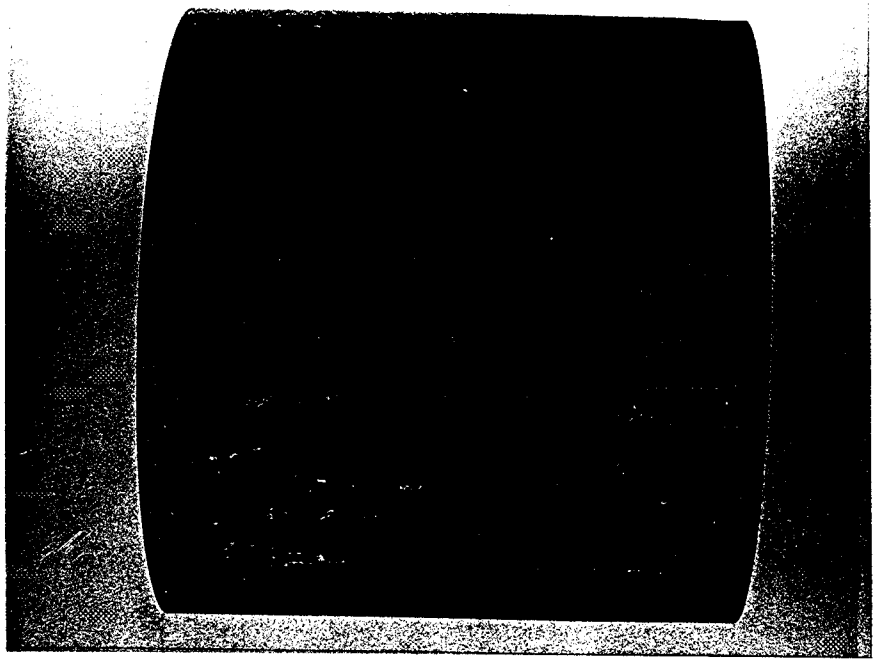

a

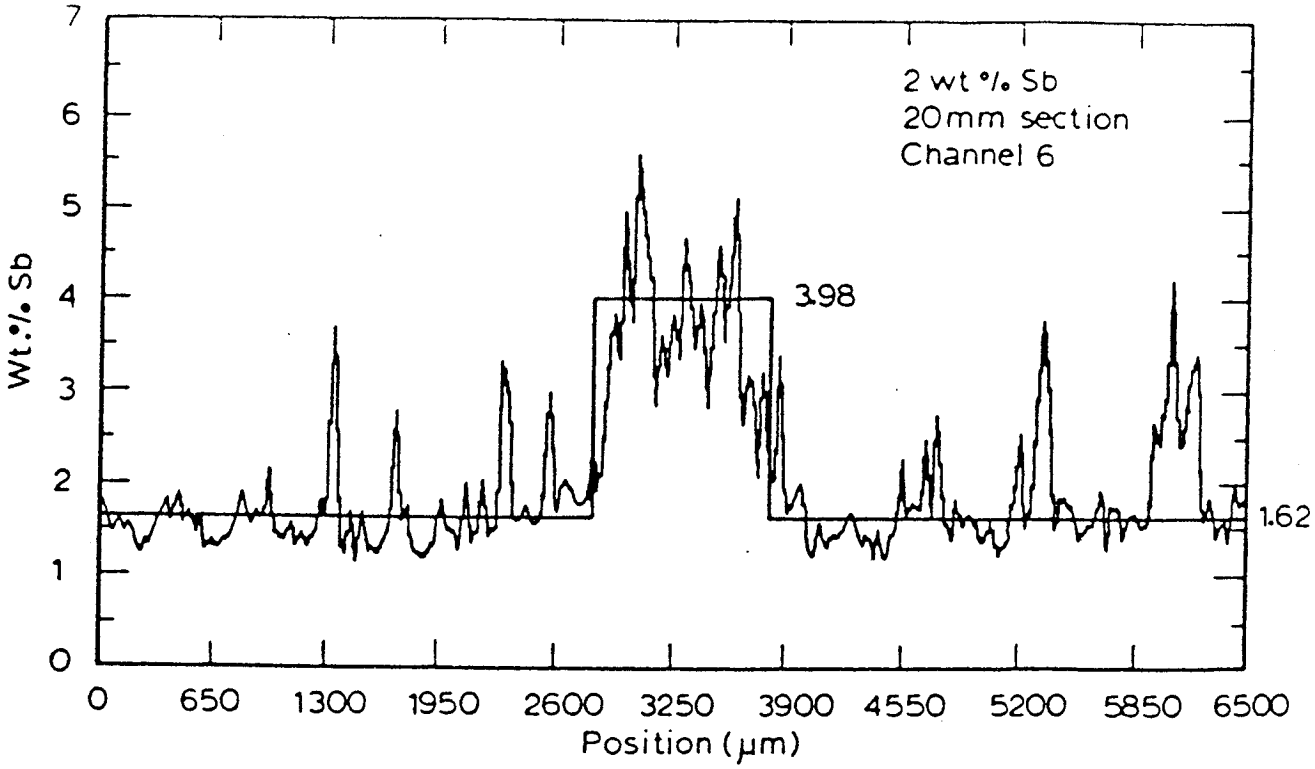
2 wt % Sb
20mm section
Channel 6
3.98
1.62
Wt.% Sb
0
1
2
3
4
5
6
7
0
650
1300
1950
2600
3250
3900
4550
5200
5850
6500
Position (μm)

b

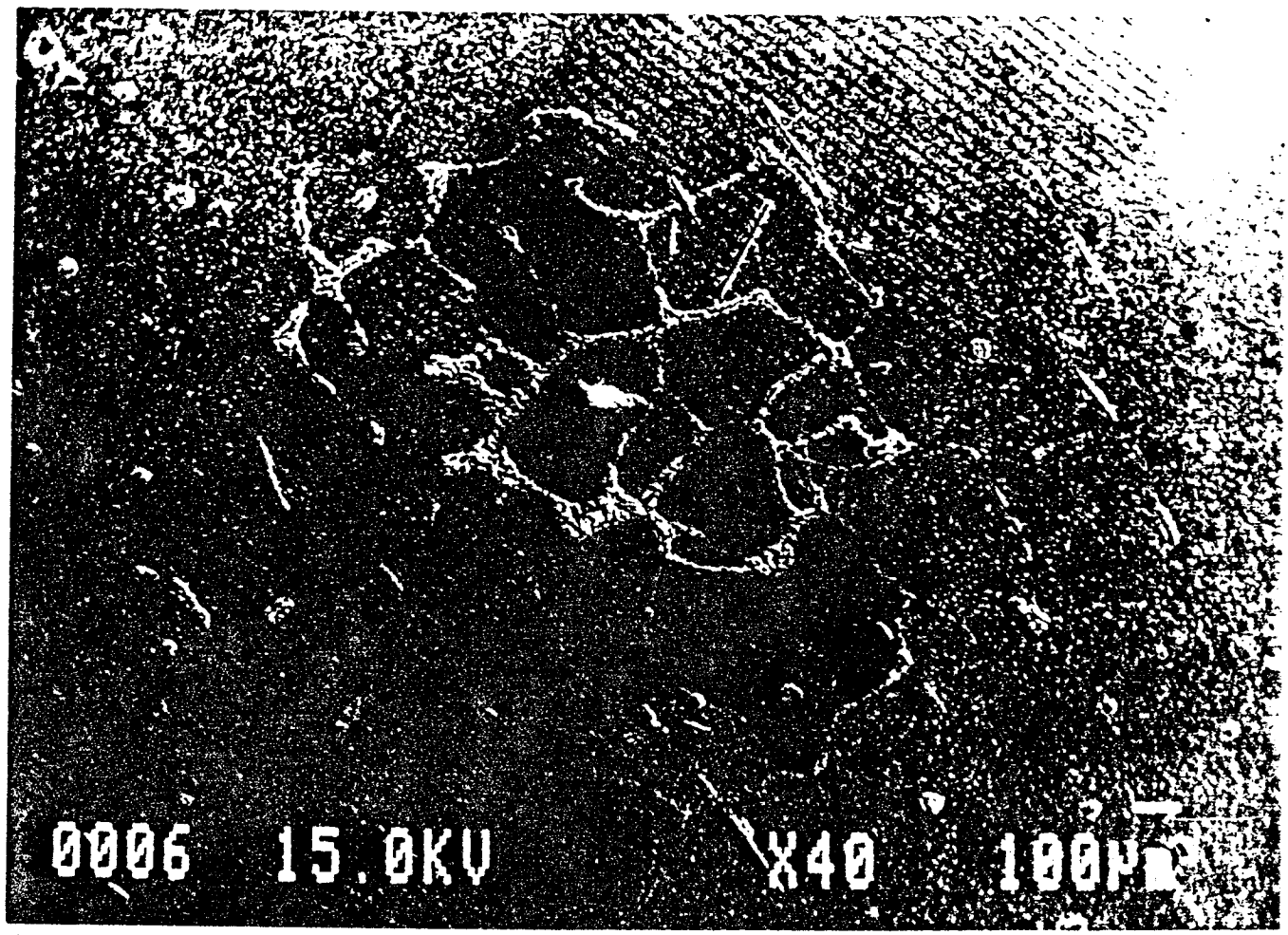
0006 15.0KV
X40
100μm

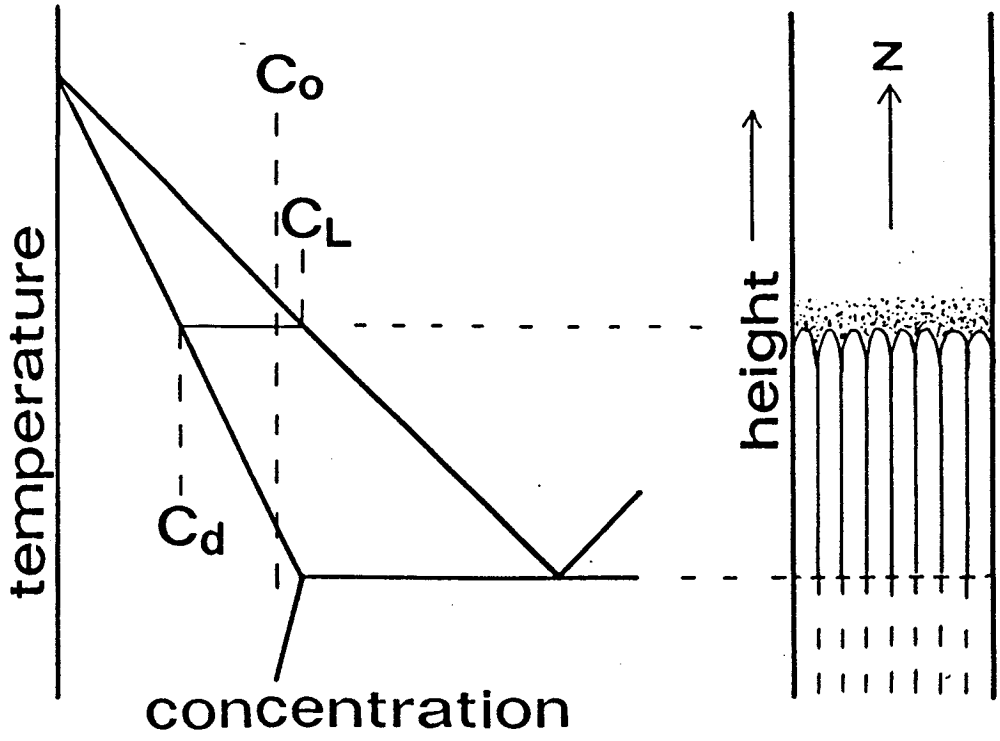
C_o
C_L
C_d
temperature
concentration
z
height

(a) (b)

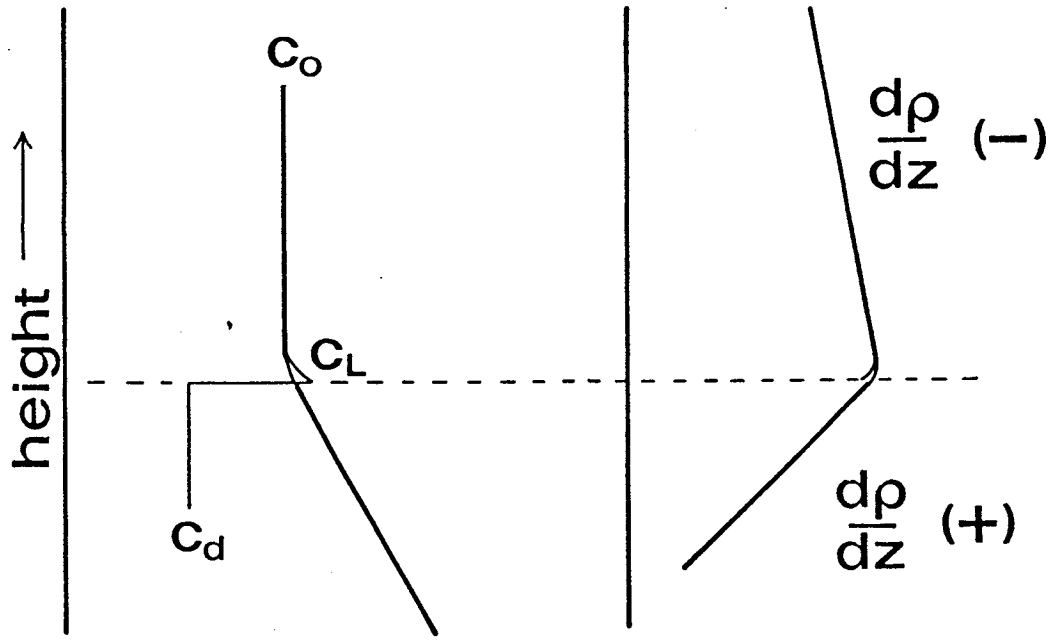
C_o
C_L
C_d
height
concentration
$\frac{d\rho}{dz}$ (−)
$\frac{d\rho}{dz}$ (+)
density

(c) (d)

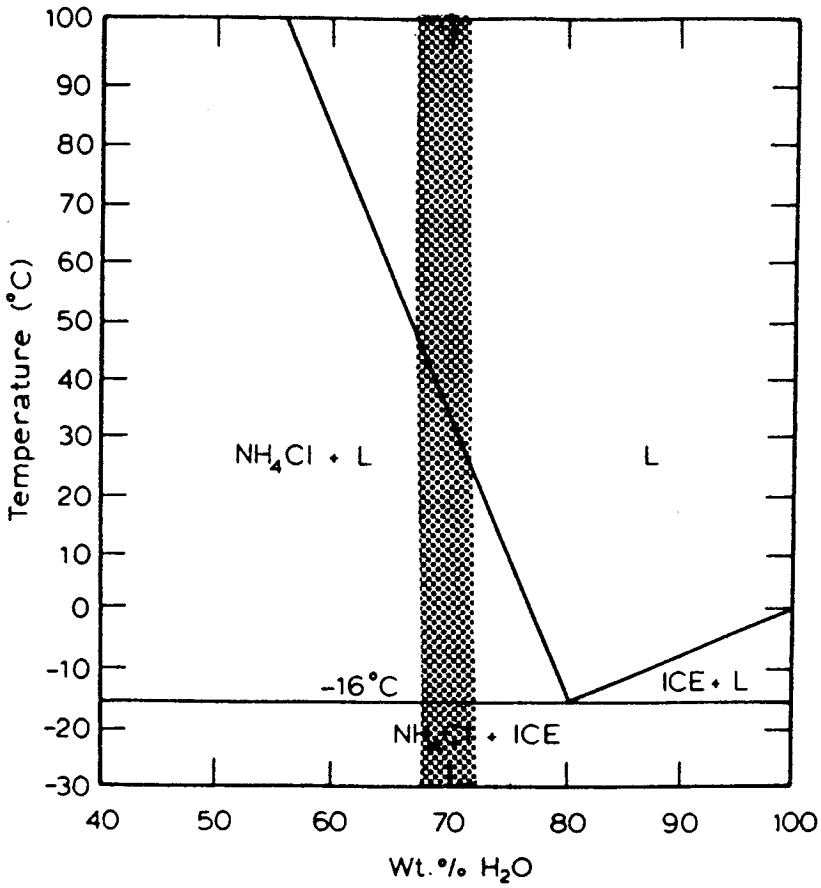
100
90
80
70
60
50
40
30
20
10
0
-10
-20
-30
Temperature (°C)
NH_4Cl + L
L
-16°C
ICE + L
NH_4Cl + ICE
40
50
60
70
80
90
100
Wt.% H_2O

OPTICAL CONFIGURATIONS

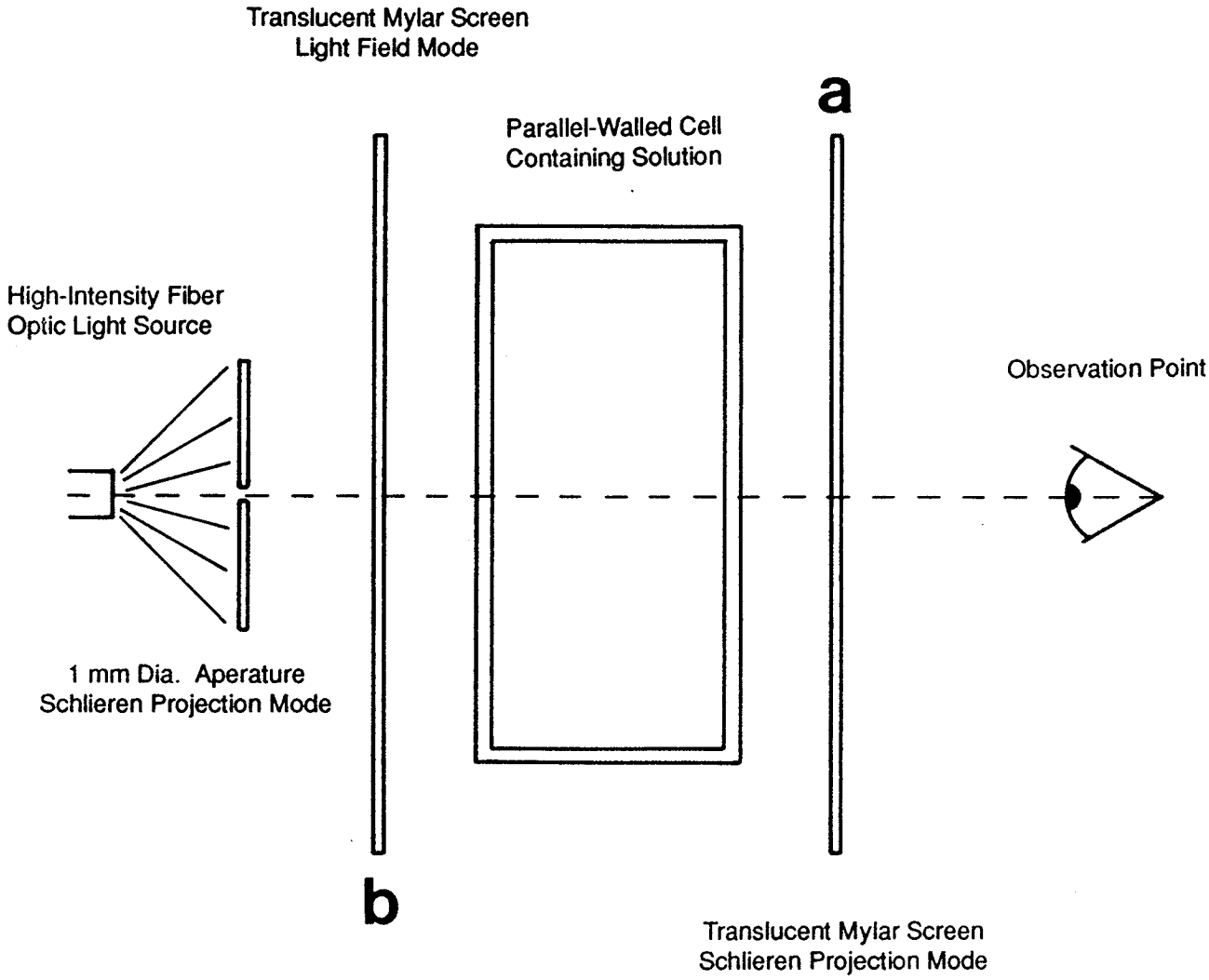

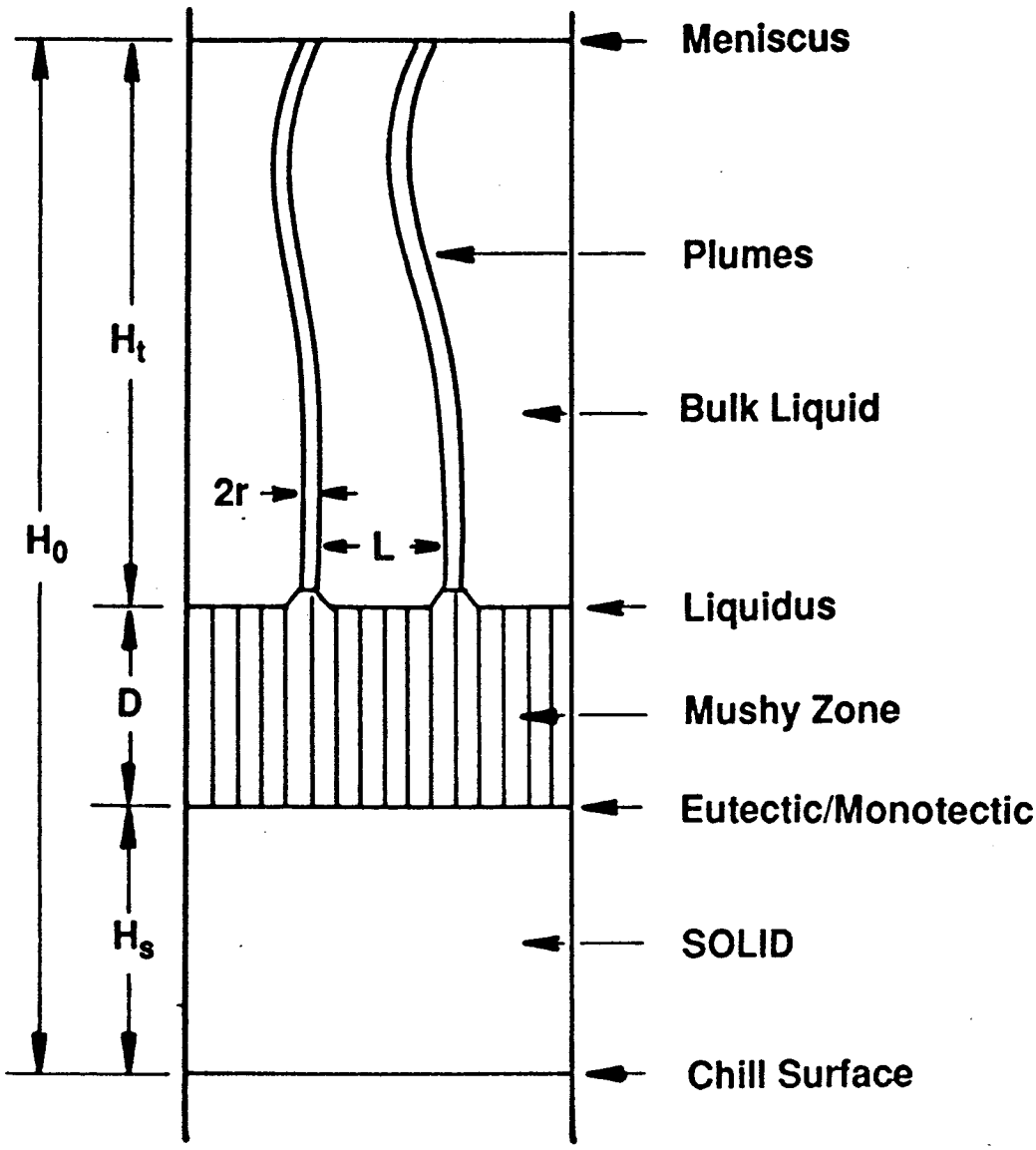
Meniscus
Plumes
Bulk Liquid
Liquidus
Mushy Zone
Eutectic/Monotectic
SOLID
Chill Surface
H_t
H_0
D
H_s
2r
L

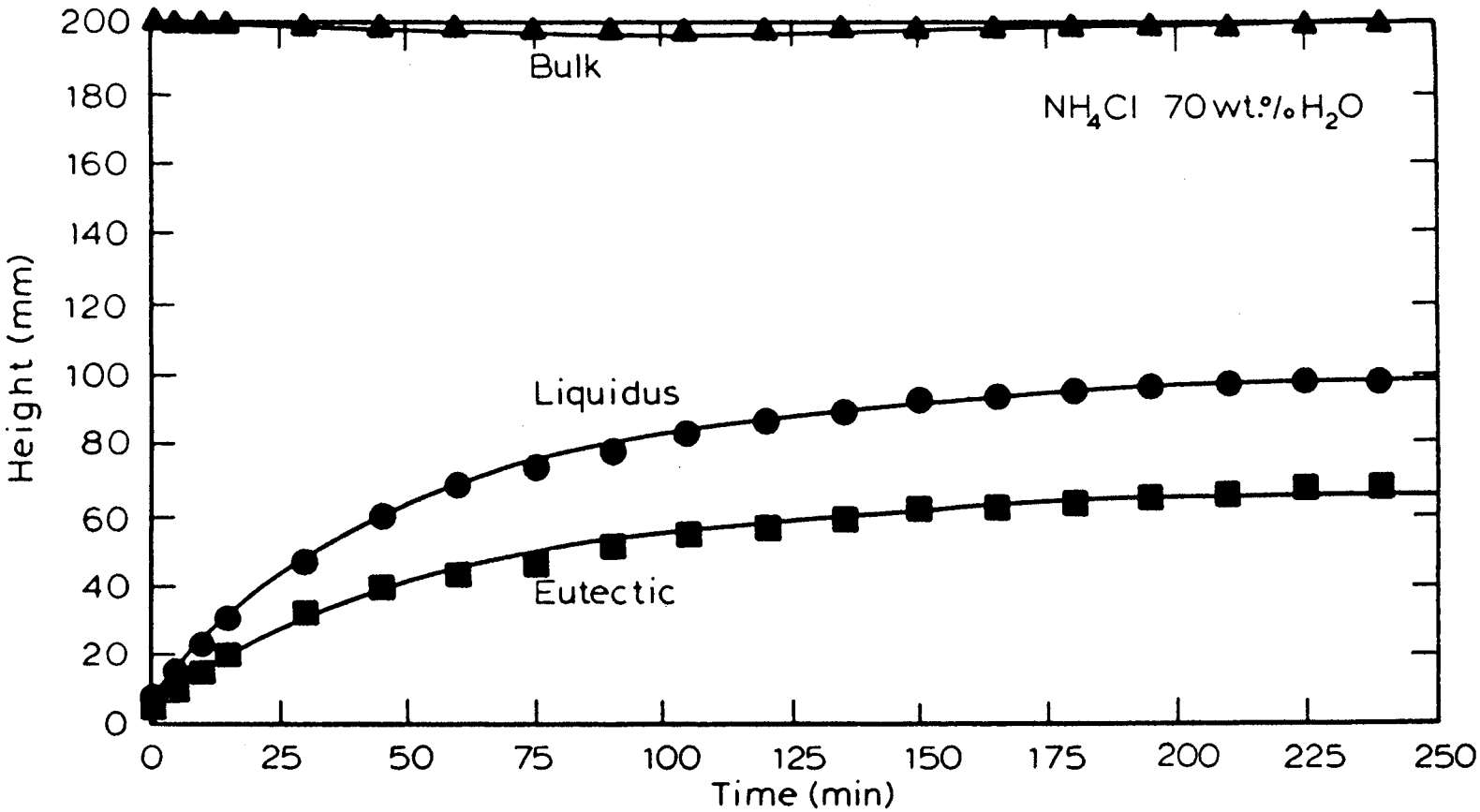
200
180
160
140
120
100
80
60
40
20
0
Height (mm)
Bulk
NH_4Cl 70 wt.% H_2O
Liquidus
Eutectic
0
25
50
75
100
125
150
175
200
225
250
Time (min)

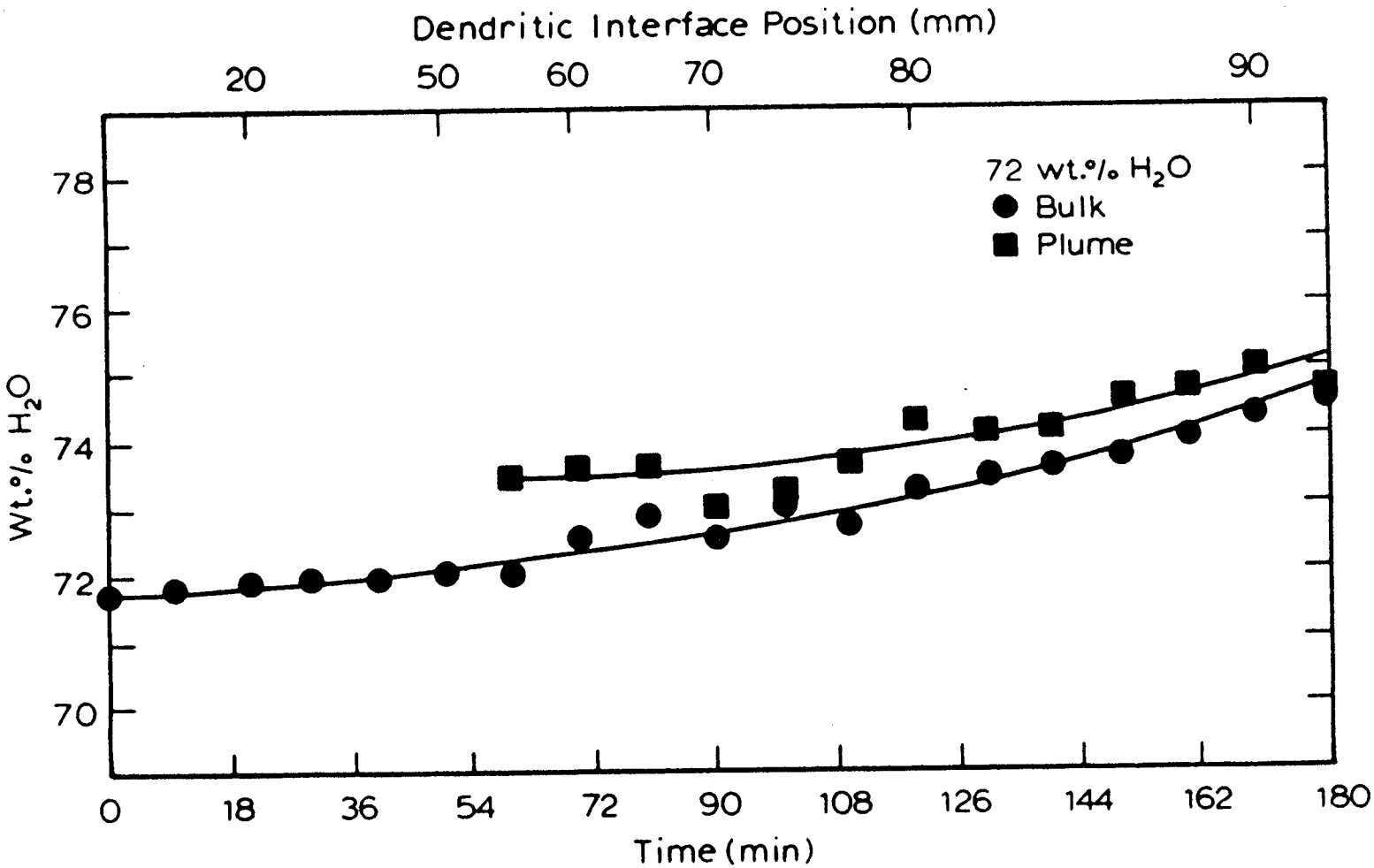
Dendritic Interface Position (mm)
20
50
60
70
80
90
72 wt.% H2O
Bulk
Plume
78
76
74
72
70
Wt.% H2O
0
18
36
54
72
90
108
126
144
162
180
Time (min)

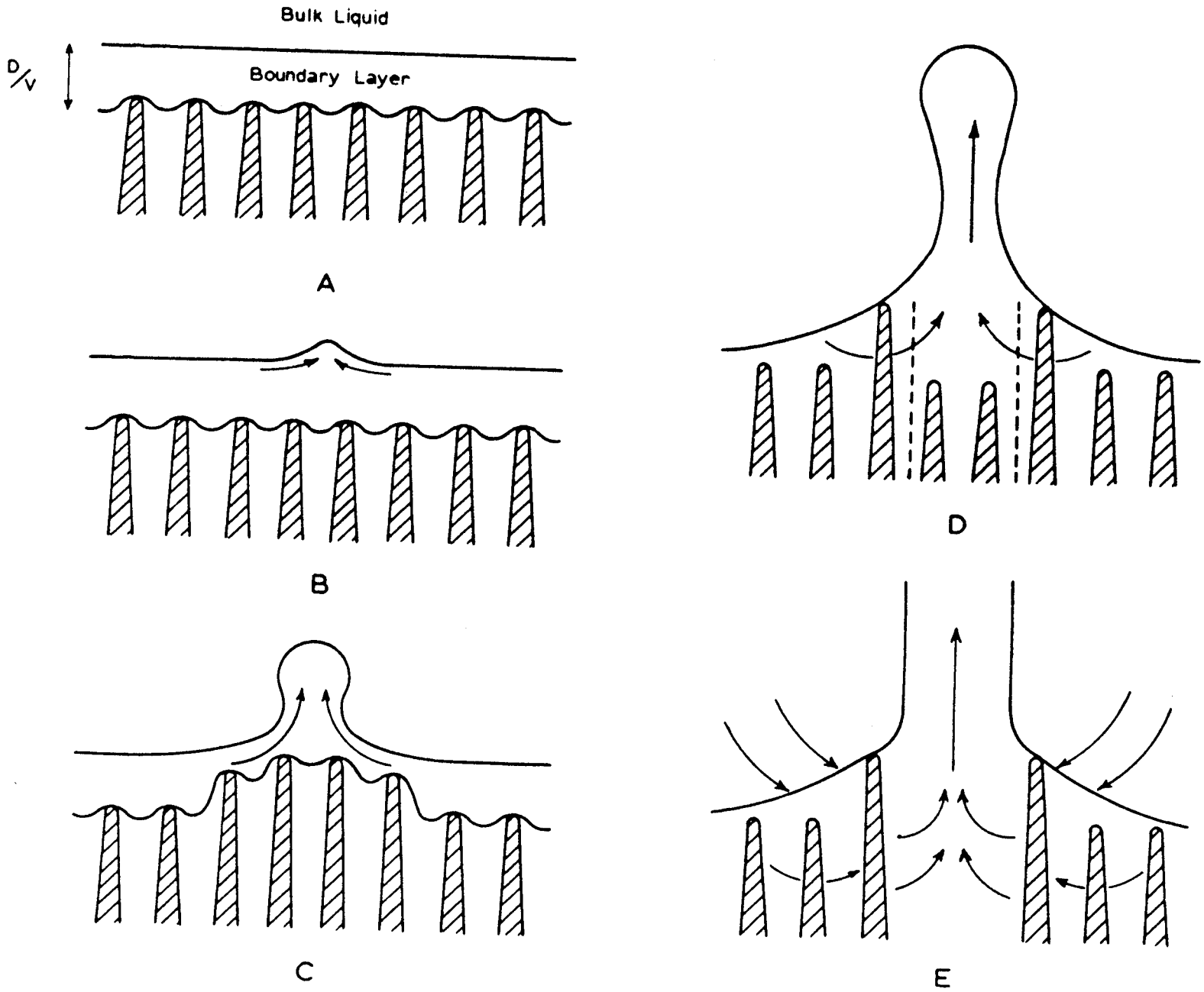
Bulk Liquid
Boundary Layer
D_V
A
B
C
D
E

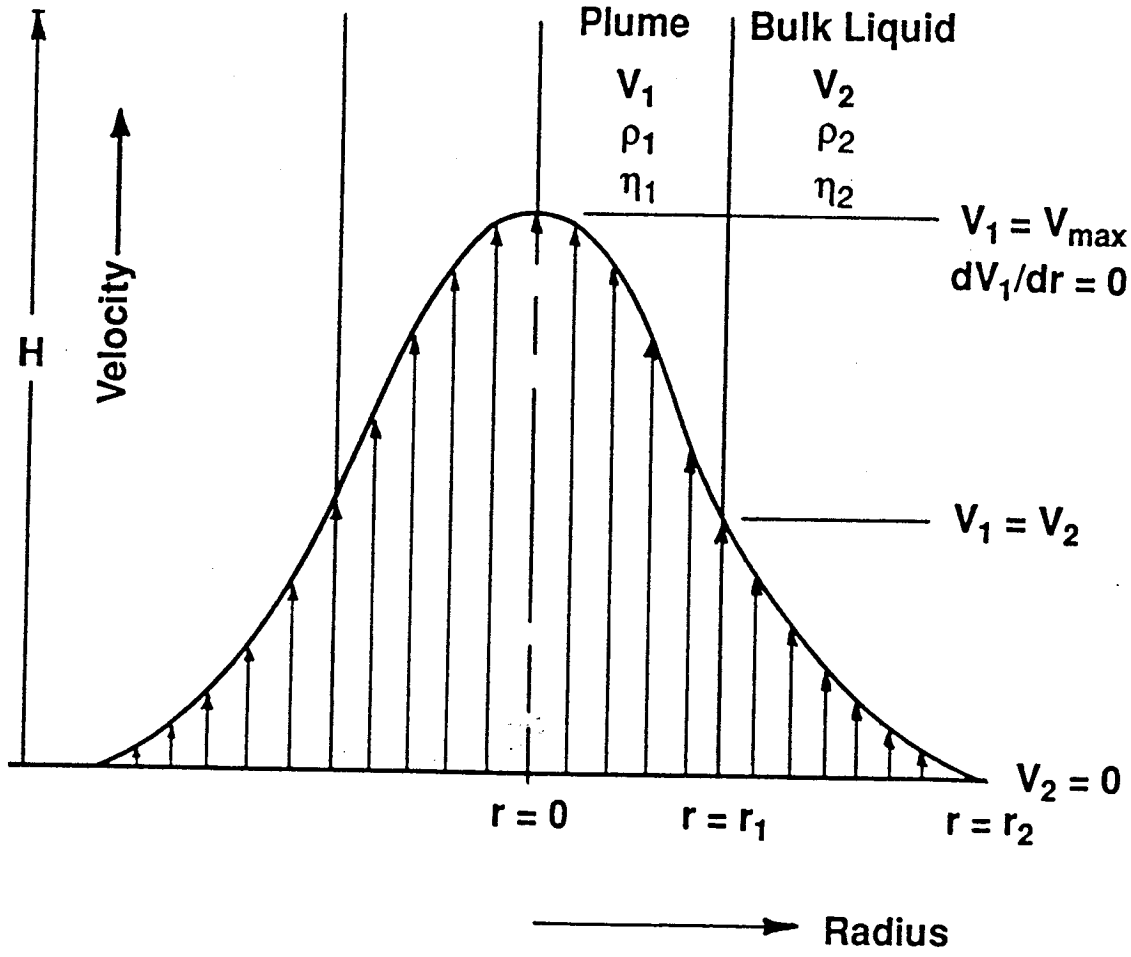
Plume
Bulk Liquid
V_1
V_2
ρ_1
ρ_2
η_1
η_2
$V_1 = V_{max}$
$dV_1/dr = 0$
H
Velocity
$V_1 = V_2$
$V_2 = 0$
r = 0
$r = r_1$
$r = r_2$
Radius